The Astrophysical Journal, 950:157 (10pp), 2023 June 20 https://doi.org/10.3847/1538-4357/accf94

Nature, Generation, and Dissipation of Alfvénic Kinks/Switchbacks Observed by Parker Solar Probe and WIND

Chuanpeng Hou[1], Xingyu Zhu[1], Rui Zhuo[1], Jiansen He[1,3], Daniel Verscharen[2], and Die Duan[1]
[1] School of Earth and Space Sciences, Peking University, Beijing, 100871, People's Republic of China; jshept@pku.edu.cn
[2] Mullard Space Science Laboratory, University College London, Dorking RH5 6NT, UK
Received 2021 October 26; revised 2023 April 13; accepted 2023 April 14; published 2023 June 20

Abstract

The discovery of very prominent magnetic kinks/switchbacks in the solar wind within 0.3 au has become a scientific highlight of the Parker Solar Probe (PSP) mission. This discovery points at the promising impact of small-scale solar activity on the inner heliosphere. To address the nature, generation, and dissipation of these kinks, we perform a statistical analysis of the plasma and boundary properties of the kinks using PSP multi-encounter observations and WIND measurements at 1 au. The kinks show strong Alfvénicity and velocity fluctuations of the order of the local Alfvén speed. These findings suggest that the nature of the kinks is consistent with large-amplitude Alfvén pulses, and the steepening of these Alfvén pulses is likely the formation mechanism of these kinks. Based on the angle between the normal direction of the kinks' boundaries and the background magnetic field vector, PSP kinks and WIND kinks can be divided into two groups: quasi-parallel and quasi-perpendicular kinks. We speculate that quasi-parallel kinks form through the coupling of Alfvén and fast waves as launched from coronal interchange magnetic reconnection. In contrast, quasi-perpendicular kinks may come from the steepening of Alfvén waves launched from both coronal interchange magnetic reconnection and from the more inhomogeneous lower solar atmosphere. We find that the kink velocity perturbation gradually decreases during outward propagation and is much lower than expected from WKB theory, suggesting a progressive dissipation of the kinks. Comparing PSP kinks and WIND kinks, we conjecture that the kinks dissipate through merging with the turbulent energy cascade within 0.25 au.

Unified Astronomy Thesaurus concepts: Solar wind (1534); Interplanetary turbulence (830); Interplanetary discontinuities (820)

1. Introduction

One of the important discoveries of PSP is the widespread existence of structured velocity spikes in the Alfvénic slow solar wind within 0.3 au (Kasper et al. 2019). These are mainly characterized by magnetic field line deflections (also known as magnetic field kinks (Tenerani et al. 2020) or switchbacks (Bale et al. 2019) and radial velocity enhancements also called velocity jets (Kasper et al. 2019) or velocity spikes (Horbury et al. 2020)), lasting from a few seconds to tens of minutes (Mozer et al. 2020). Such magnetic field kinks have attracted extensive attention due to their potential connections with solar wind acceleration and heating as well as small-scale solar activity (e.g., magnetic reconnection and wave emission; Kasper et al. 2019; Mozer et al. 2020; Dudok de Wit et al. 2020). By analyzing the pitch angle distribution of strahl electrons, Whittlesey et al. (2020) provide evidence that kink events indeed represent bends of magnetic field lines rather than current sheets. In addition to the velocity enhancements associated with magnetic field kinks, Woodham et al. (2021) find that kinks measured by PSP are also accompanied by proton temperature increases. The proton density inside the kinks is different from the density outside the kinks (Larosa et al. 2021; He et al. 2021). The magnetic field magnitude remains nearly constant except for a slight decrease at the kink boundary (Farrell et al. 2020). Magnetic field kinks have also been observed by other spacecraft beyond 0.3 au, e.g., Helios between 0.3 and 1 au (Horbury et al. 2018), ACE or WIND near 1 au (Gosling et al. 2009), and Ulysses beyond 1 au (Matteini et al. 2014). Gosling et al. (2009) report the existence of asymmetric Alfvénic fluctuations with spikes sitting on one side of such fluctuations measured by ACE near Earth. These Alfvénic velocity spikes can deform the interplanetary magnetic field into sudden kinks. However, the velocity enhancements associated with kinks in the near-Earth solar wind are less significant than the velocity enhancements associated with kinks at 0.3 au (Horbury et al. 2018). The relative changes of the average fields and plasma parameters are widely regarded as hints for theoretical and numerical predictions of the evolution of Alfvénic perturbations from the Sun into interplanetary space (Squire et al. 2020; He et al. 2021).

Two categories of possible mechanisms have been put forward to explain the origin of magnetic field kinks. The first category assumes that kinks originate from the solar atmosphere (Fisk & Kasper 2020). Magnetohydrodynamic (MHD) simulations show that the lifetime of the kink generated by interchange magnetic reconnection in the corona is typically longer than the propagation time of the kinks from the solar corona to PSP (Tenerani et al. 2020). He et al. (2021) propose a new coronal interchange reconnection model with a guide-field discontinuity that generates Alfvénic pulses due to the release of the discontinuous guide-field component. In their model, both fast-mode and slow-mode magnetosonic waves are launched simultaneously with the Alfvén pulses due to the

[3] Corresponding author.

penetration of reconnection-induced plasmoids into the ambient open field region. He et al. (2021) further find that the sampling sequences of the modeled kinks are qualitatively consistent with PSP observations in terms of magnetic field, plasma flow velocity, temperature, and density. Zank et al. (2020) analyze the evolution equation of radial magnetic field deflection structures, which may be generated at an interchange reconnection site and propagate at the fast magnetosonic speed. In this model, the fast-wave mode is responsible for the formation of switchback structures. A statistical analysis based on one-humped kinks during PSP's first solar encounter also supports the generation of kinks from interchange magnetic reconnection (Liang et al. 2021). Horbury et al. (2020) find that the kinks in two solar wind streams at different heliocentric distances have similar structures, which may be evidence for their common solar origin. Moreover, in the statistical work of Dudok de Wit et al. (2020), the PSP kinks have long-range correlations independent of the background solar wind, supporting the hypothesis of a solar origin of the kinks. In an alternative explanation framework, the kinks are assumed to be generated locally in the solar wind (Matteini et al. 2014; Squire et al. 2020). Squire et al. (2020) propose, based on compressible MHD simulation results, that locally formed Alfvénic fluctuations evolve into kinks by radial expansion, whereby strong magnetic field kinks represent tangential discontinuities (TD). Kinks may also arise from the perturbations of magnetic field lines caused by stream interactions. In MHD simulations, nonlinear shear-driven turbulence also produces kink fluctuations under certain circumstances (Ruffolo et al. 2020). The foot point of a magnetic field line jumps from a low-speed flow zone to a high-speed flow zone, forming a super-Parker spiral that might produce a kink beyond the Alfvén critical point (Schwadron & McComas 2021). Since the community has not reached a consensus regarding the origin of magnetic field kinks, multi-spacecraft observations of their statistical properties can provide further insight.

One possible reason for the increased temperature inside the kinks is the dissipation of kinks during their outward propagation. Froment et al. (2021) report magnetic reconnection at the kink boundaries, indicating that the reconnection events triggered at the kink boundaries may lead to the dissipation of the kinks and transfer energy from kinks to the solar wind particles. However, based on observations during the first solar encounter (E1) of PSP, most of the kink boundaries can be seen as rotational discontinuities (RD-type kinks), and a small proportion of kink boundaries show the properties of tangential discontinuities (TD-type kinks; Larosa et al. 2021). Liu et al. (2022) count the interplanetary discontinuities observed by PSPs within 0.3 au and show that 73% of 3948 interplanetary discontinuities are rotational discontinuities. Since rotational discontinuities (RDs) can originate from the steepening of large-amplitude Alfvén waves (Tsurutani et al. 1994; Yang et al. 2015), the statistical results of Liu et al. (2022) support the idea that the Alfvénic turbulent environment near the Sun is indeed more suitable for the generation of RDs. Hence, magnetic reconnection is not necessarily the primary mechanism to explain the dissipation of the kinks. However, compared to TDs and magnetic reconnection, RDs are usually not accompanied by significant particle heating (Wang et al. 2013). Therefore, the mechanism responsible for the enhanced temperature inside the kinks remains to be identified. In the statistical work of Huang et al. (2020), the solar wind observed by PSP reveals a nonadiabatic expansion, consistent with its ongoing heating during the expansion which is more pronounced within 0.3 au. Therefore, the relationship between the solar wind heating mechanism within 0.3 au and the prevalence of kinks within 0.3 au is a topic worth investigating.

In this work, using PSP and WIND measurements, we study the properties of kinks based on the magnetic field and plasma properties across their boundaries, investigate the differences, and discuss the implication for our understanding of the generation and evolution of the kinks. This paper is organized as follows: In Section 2, we introduce the data from PSP and WIND. In Section 3, we show our statistical results for PSP kinks and WIND kinks. In Section 4, we discussion the generation and dissipation of the kinks. Section 5 is our summary.

2. Data

We analyze 10 days of measurements around each PSP perihelion during nine solar encounters (1, 2, 4, 5, 6, 7, 8, 9, and 10), as highlighted by the red segments in Figure 1(a). We show the probability density function (PDF) of PSP's heliocentric distance during the time intervals of the data set used in this work in Figure 1(b). Every 6 hours, we calculate the angle ($\theta_{\rm BR}$) between the local magnetic field vector and the radial direction. We take the median value of $\theta_{\rm BR}$ during each encounter interval as the background value ($\theta_{\rm BR,0}$). Then we obtain a time series of the angle deflection $\delta\theta_{\rm BR}$ defined as $\theta_{\rm BR}-\theta_{\rm BR,0}$. To identify magnetic kinks, we use the condition of $\delta\theta_{\rm BR}>25^\circ$ as the selection threshold, and the duration needs to be more than 60 s. For kinks with different magnetic angle deflections, the distributions of kink waiting time and duration are remarkably similar (Dudok de Wit et al. 2020). Hence, we expect that kinks with a long duration reappear after a longer waiting time. For kinks lasting more than 60 s, we estimate the waiting time to be 120 s, based on the distributions of kink waiting time and duration shown by Dudok de Wit et al. (2020). We notice that the time interval between some preliminary selected kink events is relatively short (typically less than 120 s). To facilitate subsequent calculation and analysis, we group the events with waiting times of less than 120 s as a single event of a longer duration. Using this method and the magnetic field measurements from PSP's flux-gate magnetometer (MAG; Bale et al. 2016), we obtain a total of 866 kink events. We statistically analyze the plasma number density, bulk velocity, and temperature inside and outside the kink events in the RTN coordinate system, where R points from the solar center to the spacecraft, T results from the cross product of the solar rotation vector with the R direction, and N serves as the third axis to complete the right-handed coordinate system. We use the fitted data from the Solar Probe Cup (SPC; Kasper et al. 2016) for the radial component of solar wind flow velocity and turn to SPAN-i data to supplement the time segments lacking radial velocity measurements from SPC. For the other two components of the solar wind velocity, the number density, and the temperature, we use the data provided by SPAN-i. The sampling frequency of the magnetic field is 293 Hz, and the cadence of data provided by SPC and SPAN-i is about 0.8 s and 3.5 s, respectively.

For our WIND observations during the whole year of 2012, we manually select a set of events consisting of 58 kinks. Our primary selection criterion is a sharp change of the angle between the average magnetic field and the radial direction by at least 15°. For obtaining a sufficient number of WIND kinks,

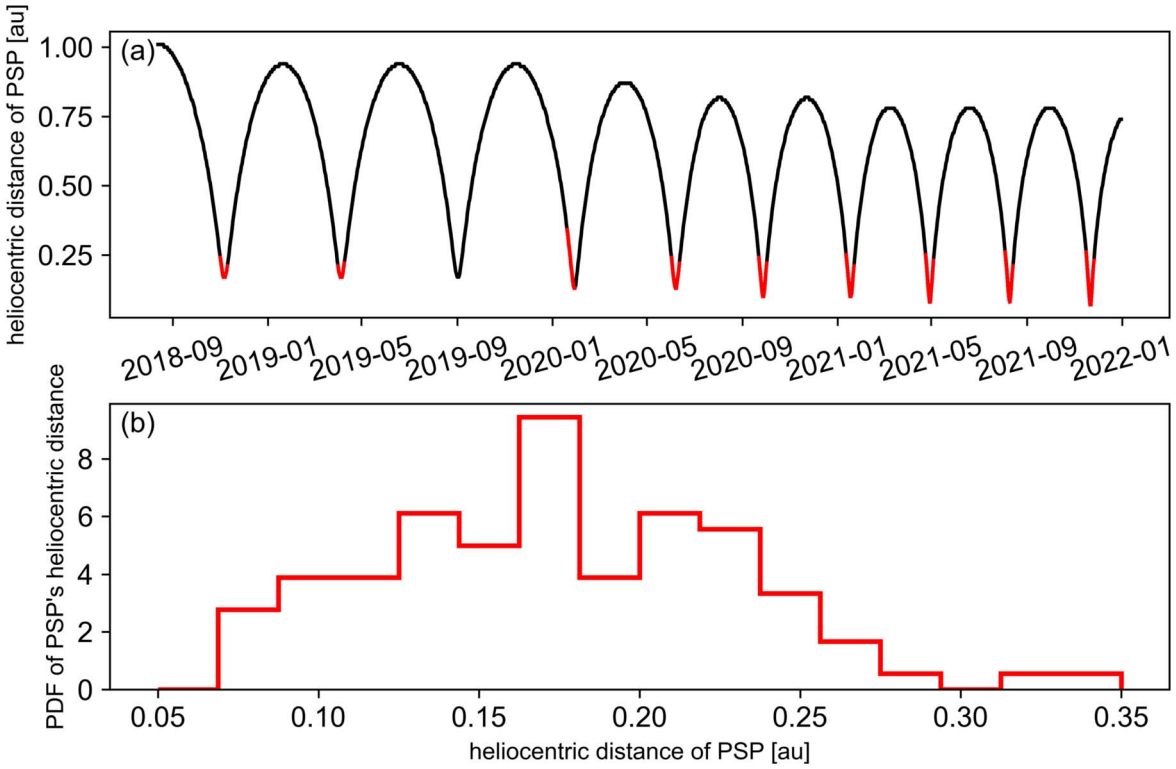

Figure 1. (a) The black line shows the heliocentric distance of Parker Solar Probe (PSP) during the first 10 solar encounters. The red segments represent the time intervals of the PSP data set used in this work. (b) The probability density function (PDF) of the heliocentric distance of PSP during the time intervals marked by the red segments in the top panel.

the threshold (15°) is lower than that (25°) for PSP kinks. Moreover, we only select time intervals during which the pitch angle polarity of the strahl electrons does not change across the kinks to eliminate the possibility of field direction change due to interplanetary current sheet crossings. For every kink event, there are a pair of kink boundaries separating kink and background plasma. We analyze the magnetic field and plasma data supplied by the Magnetic Field Investigation (MFI; Lin et al. 1995) and the Three-dimensional Plasma Analyzer (3DP; Lepping et al. 1995). We use the magnetic field and plasma data at a low cadence of 92 s to calculate average quantities. For calculating the correlation coefficients between magnetic field and plasma bulk velocity, we adopt the magnetic field and plasma data at a higher cadence of 3 s.

3. Results

3.1. Plasma Properties of PSP Kinks and WIND Kinks

Figures 2(a)–(c) show the main properties used to characterize and identify kinks: a significant rotation of the magnetic field at mostly constant magnetic field magnitude, leading to a significant variation of the radial magnetic field inside the kinks. Each point in these panels corresponds to a PSP-kink event, and the colors denote the heliocentric distance of each event. The magnetic field strength around the PSP kinks increases as the heliocentric distance decreases. According to our statistical study, there is no clear heliocentric distance dependence of the change of θ_{BR} associated with the PSP kinks. There is a clear difference in the plasma properties inside and outside the PSP kinks, which evolves with heliocentric distance. We find a velocity increase inside the PSP kinks (Figure 2(d)), and the velocity increase is more pronounced for kinks closer to the Sun, indicated by the red points being farther away from the diagonal line in Figure 2(d). The velocity difference between inside and outside the Alfvénic kinks corresponds approximately to the local Alfvén speed. As the heliocentric distance decreases, and thus the local Alfvén speed increases, we find a higher velocity increase inside the kinks. In addition to the velocity increase, most PSP-kink events possess a decrease in density (Figure 2(e)) and an increase in temperature (Figure 2(f)). Closer to the Sun, the decrease in density and increase in temperature within the kink are more pronounced.

To obtain the radial trend of the differences between inside and outside the PSP kinks, we calculate and illustrate the distributions of the following three variables: $\delta V_r/V_{A,out} = (V_{r,in} - V_{r,out})/V_{A,out}$; $\delta N_p/N_{p,out} = (N_{p,in} - N_{p,out})/N_{p,out}$; and $\delta T_p/T_{p,out} = (T_{p,in} - T_{p,out})/T_{p,out}$, where V_r, $V_{A,out}$, N_p, and T_p are the radial solar wind speed, Alfvén speed, proton number density, and proton temperature; and the subscripts "in" and "out" refer to inside and outside the kinks, at different heliocentric distances (Figure 3). We calculate normalized values to eliminate the impact of the radial of the background density and background temperature on the statistical results. In Figure 3, each point corresponds to a kink event, and its color indicates the concentration level of kink events in the parameter space, where the yellow color means that more points are concentrated around that point. On the right-hand side of each panel, we provide the distribution of the three variables ($\delta V_r/V_{A,out}$, $\delta N_p/N_{p,out}$, $\delta T_p/T_{p,out}$) for events at all measurement distances. The locations of the peaks in these three histograms, which are well away from the zero level, indicate on average increasing velocity, decreasing density, and increasing temperature inside the kinks compared to the background plasma outside.

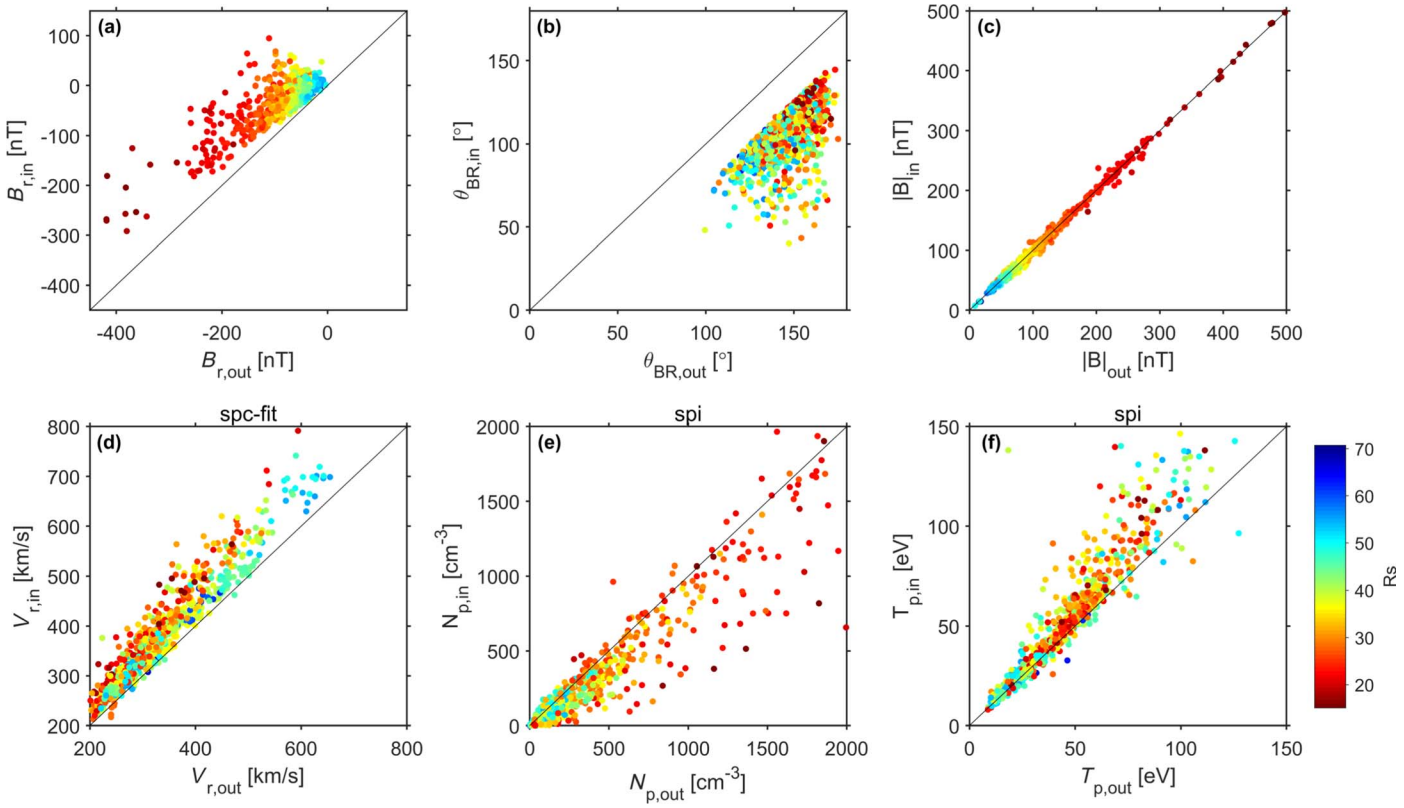

Figure 2. Scatterplots of averaged properties inside (in) and outside (out) the PSP kinks. (a) Radial component of the magnetic field (B_R). (b) Angle between the mean magnetic field direction and the radial direction (θ_{BR}). (c) Magnitude of the magnetic field ($|B|$). (d) Radial component of the proton bulk velocity (V_r). (e) Proton number density (N_p). (f) Proton temperature (T_p). The color of each point represents the heliocentric distance.

According to the distributions of points and the histograms, the relative changes in velocity and density distribute over a wider range than in temperature. The histogram on the top of Figure 3(a) shows the distribution of kink events over heliocentric distances. This histogram shows a peak around 0.17 au, probably due to the distribution of the original data set across heliocentric distances, which is displayed in Figure 1. In each heliocentric distance bin, we calculate the averages and standard deviations of the three quantities for all kink events, marked as white dashed lines with error bars.

We apply a fitting function to approximate the basic distance trend of the scatter points in Figure 3, and plot the fitted curves for the three variables versus heliocentric distance (red lines in Figure 3). When fitting the scatter plot in Figure 3(c), we do not include outliers of kink events with $\delta T_p/T_{p,out} > 0.50$, which otherwise cause the fitting result to deviate from the main trend. Both the red fitted curves and the white dashed lines match well the main trends in the three panels. According to the fitted curve, the normalized difference between the velocity inside and outside the kinks (Figure 3(a)) gradually decreases with increasing heliocentric distance and eventually flattens. This suggests that, at least within 0.25 au, the velocity enhancements inside kinks decrease gradually along with the kinks' outward propagation, rather than remaining at the local Alfvén speed. WKB theory predicts that the normalized velocity fluctuations of outward Alfvén waves decrease with heliocentric distance r as $\delta V/V_A \sim \delta B/B_0 \sim \frac{r^{-1.5}}{r^{-2}} \sim r^{1/2}$, where B_0 corresponds to background magnetic field (Tu & Marsch 1995). It is clear that our fitted curve is significantly below the predictions of the WKB theory (blue line in Figure 3(a)). This trend suggests the existence of an energy dissipation processes for kink events during their outward propagation, which converts energy associated with the kinks to other types of energy. We discuss the dissipation process of kinks specifically in Section 4. The fitted curve in Figure 3(b) shows that the density difference inside and outside the kinks decreases with increasing heliocentric distance. In Figure 3(c), closer to the Sun, the proton temperature increases associated with kinks are more pronounced. We consider the increased proton temperature inside the kinks an effect of the kink dissipation.

To verify the reliability of the selected WIND kinks, we also show the distribution of the magnetic field properties inside and outside the WIND kinks in Figures 4(a)–(c). We again focus on the plasma properties inside and outside the kinks. Inside the WIND kinks, the velocity increase is insignificant. The velocity difference is about 10 km s^{-1}, which is about one-fifth of the average local Alfvén speed at 1 au. This ratio of 0.2 between the velocity difference and the local Alfvén speed is consistent with the asymptotic trend of the fitted curve in Figure 3(a). It also indicates that the ratio of increased velocity inside the kinks to the Alfvén velocity is relatively constant between 0.25 and 1 au, and the energy dissipation of kinks is mainly concentrated within 0.25 au. There are no significant differences in density (Figure 4(e)) and temperature (Figure 4(f)) inside and outside the WIND kinks, which is consistent with the asymptotic trend of the fitted curves in Figures 3(b) and (c).

3.2. Alfvénicity inside and outside Kinks

The theory of wave propagation in inhomogeneous media predicts that the steepening of Alfvén waves during outward propagation can form kinks, even switchback geometries

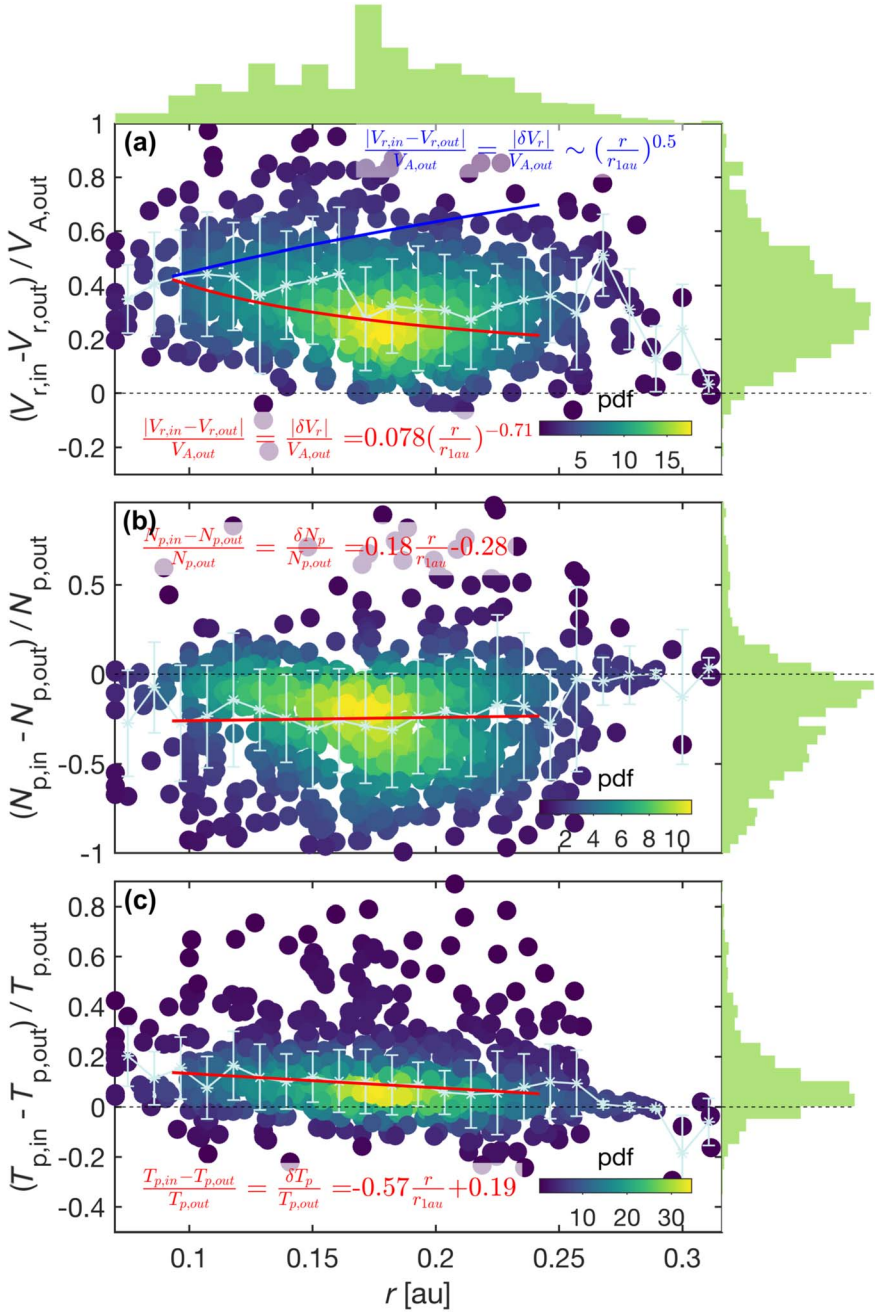

Figure 3. Distribution of kinks in the 2D parameter space of plasma properties and heliocentric distance. (a) Distribution of kinks in the 2D space of $(V_{r,in} - V_{r,out})/V_{A,out}$ and heliocentric distance. (b) Distribution of kinks in the 2D space of $(N_{p,in} - N_{p,out})/N_{p,out}$ and heliocentric distance. (c) Distribution of kinks in the 2D space of $(T_{p,in} - T_{p,out})/T_{p,out}$ and heliocentric distance. On the right-hand side of the three panels, the histograms show the distributions of $\delta V_r/V_A$, $\delta N_p/N_{p,out}$, and $\delta T_p/T_{p,out}$ for the kink events. On the top of panel (a), the histogram shows the distribution of heliocentric distances for the kink events. The black dashed lines correspond to the locations where the three parameters are zero.

(Squire et al. 2020). Based on this theory, we expect similar Alfvénicity inside and outside kink events in the Alfvénic solar wind. In Figure 5, we show the correlation between the magnetic field vector components and velocity vector components of PSP kinks and WIND kinks. The distributions of correlation coefficients inside and outside the kinks are not significantly different, and the peaks of the distributions are close to 1. These peaks indicate that kinks indeed possess strong Alfvénicity. However, in terms of the spread of the distribution, more PSP kinks have lower Alfvénicity compared to WIND kinks. We speculate that the PSP kinks of low Alfvénicity result from partial dissipation during their outward propagation and may be less likely to maintain their Alfvénicity when approaching 1 au. Shi et al. (2022) find that switchbacks distribute in clusters and that the Alfvénicity of the switchback clusters is higher than in the background quiet solar wind. Their result differs from ours of similar Alfvénicity inside and outside the observed kinks. Both results can be reconciled by the scenario of kink formation through the steepening of Alfvén waves. If an Alfvén wave train steepens to form multiple kinks, numerous kinks within this wave train form a cluster of switchbacks. In this case, there would be a difference in Alfvénicity between the switchback cluster and the quiet solar wind. When we discuss the Alfvénicity inside and outside

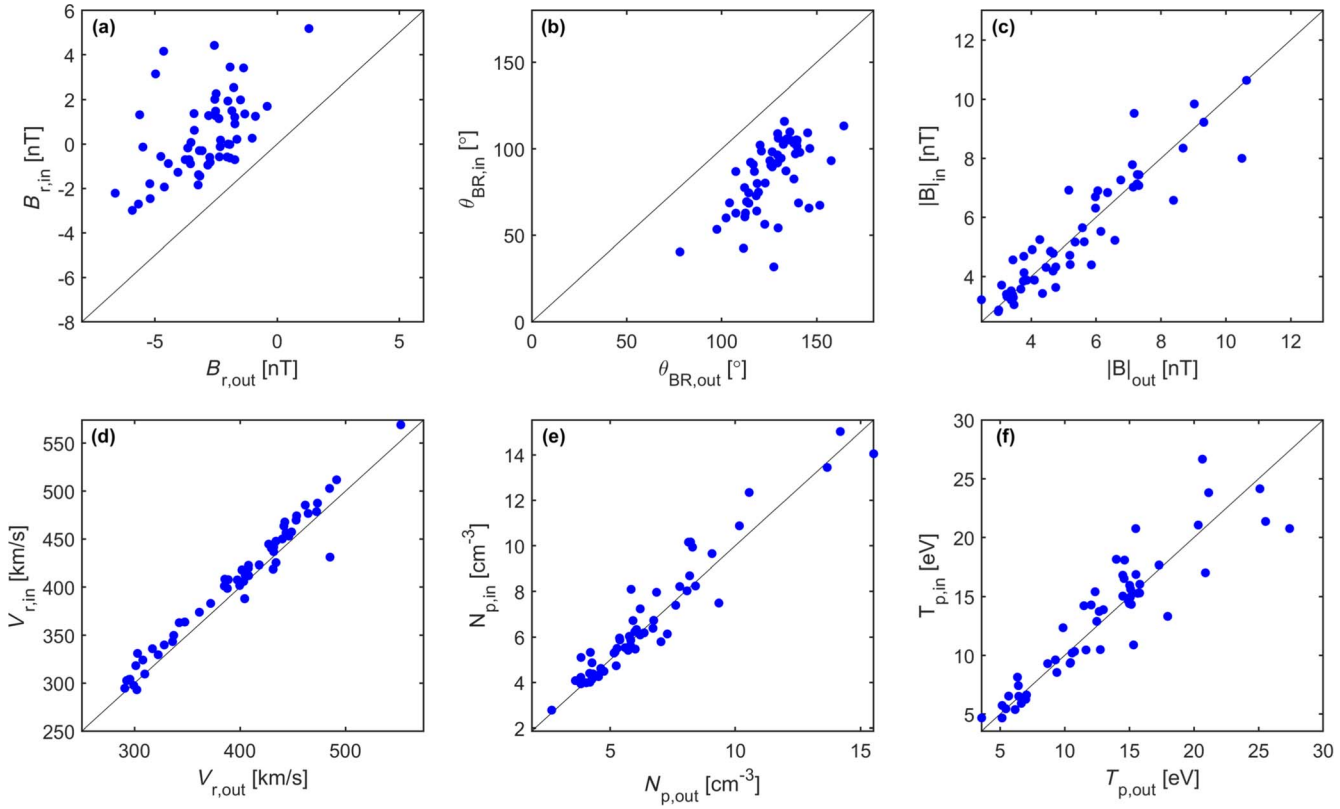

Figure 4. Scatterplots of averaged properties inside (in) and outside (out) the WIND kinks. All points are recorded at a heliocentric distance of ∼1 au. The layout of this figure is similar to that of Figure 2. (a) Radial component of the magnetic field (B_R). (b) Angle between the mean magnetic field direction and the radial direction (θ_{BR}). (c) Magnitude of the magnetic field ($|B|$). (d) Radial component of the proton bulk velocity (V_r). (e) Proton number density (N_p). (f) Proton temperature (T_p).

a kink event within a cluster of kinks/switchbacks, since phase steepening is located in the interior of the wave train, there would be no significant difference of Alfvénicity between inside and outside a single kink event. In this interpretation, magnetic kinks/switchbacks would be a consequence of Alfvén wave steepening.

3.3. Discontinuity Types and Normal Directions of Kink Boundaries

In the de Hoffman–Teller (HT) reference frame, we calculate the Pearson correlation coefficient (CC) between the radial magnetic field component and the radial velocity component on both sides of the kink boundary. We use $CC > 0.8$ as a reliable criterion for judging a kink boundary as an RD. In Figure 6, we provide the percentage of PSP kinks and WIND kinks with RD-type boundaries at different heliocentric distances. We do not observe a dependence of the percentage of RD-type kinks in the PSP data set on heliocentric distance. The percentage of RD-type PSP kinks is about 58%, and the percentage of RD-type WIND kinks is slightly higher at about 69%. Therefore, the majority of PSP kinks and WIND kinks belong to the RD type. In addition, the slightly higher percentage of RD types in WIND kinks suggests that kinks of non-RD type may be more likely to dissipate during the outward propagation.

For each kink, we employ the Minimum Variance Analysis (MVA) method (Sonnerup & Scheible 1998) to estimate the normal direction of the boundary and calculate the angle θ_{Bn} between the normal direction and the background magnetic field. Figures 7(a) and (b) show the distributions of θ_{Bn} for PSP kinks and WIND kinks, respectively. We find that PSP kinks and WIND kinks can be divided into two groups: quasi-parallel kinks (blue region) and quasi-perpendicular kinks (gray region). For the PSP kinks, the proportion of quasi-parallel kinks is significantly higher than that of quasi-perpendicular kinks. On the other hand, the proportions of both groups are approximately equal for the WIND kinks. The two-group distribution of kink events also exists at different heliocentric distances (Figure 7(c)). The number of quasi-parallel kinks decreases more rapidly with increasing heliocentric distance, resulting in a similar number of quasi-parallel and quasi-perpendicular kinks at larger distances from the Sun. This finding suggests the quasi-parallel kinks may suffer stronger dissipation. In Figure 7(d), we illustrate the number of RD (red bars) and non-RD (blue bars) events as functions of θ_{Bn}. The black line is the percentage of RDs. For the quasi-parallel kinks, the percentage of RDs increases as θ_{Bn} increases, while for the quasi-perpendicular kinks, the percentage of RDs remains constant. A possible explanation is that a quasi-parallel RD-type kink with large θ_{Bn} may be more stable, and the stability of RD-type kinks for quasi-perpendicular events is unrelated to θ_{Bn}.

4. Discussion

Based on our set of kink events, our statistical results are consistent with the idea of kink formation through the steepening of Alfvénic pulses. However, the solar source of these Alfvén pulses is still unclear. One scenario proposes that Alfvén pulses are excited by coronal interchange magnetic reconnection (e.g., He et al. 2021). Another scenario proposes that the Alfvén pulses originate from the reshuffling of magnetic line footpoints in the photosphere due to plasma

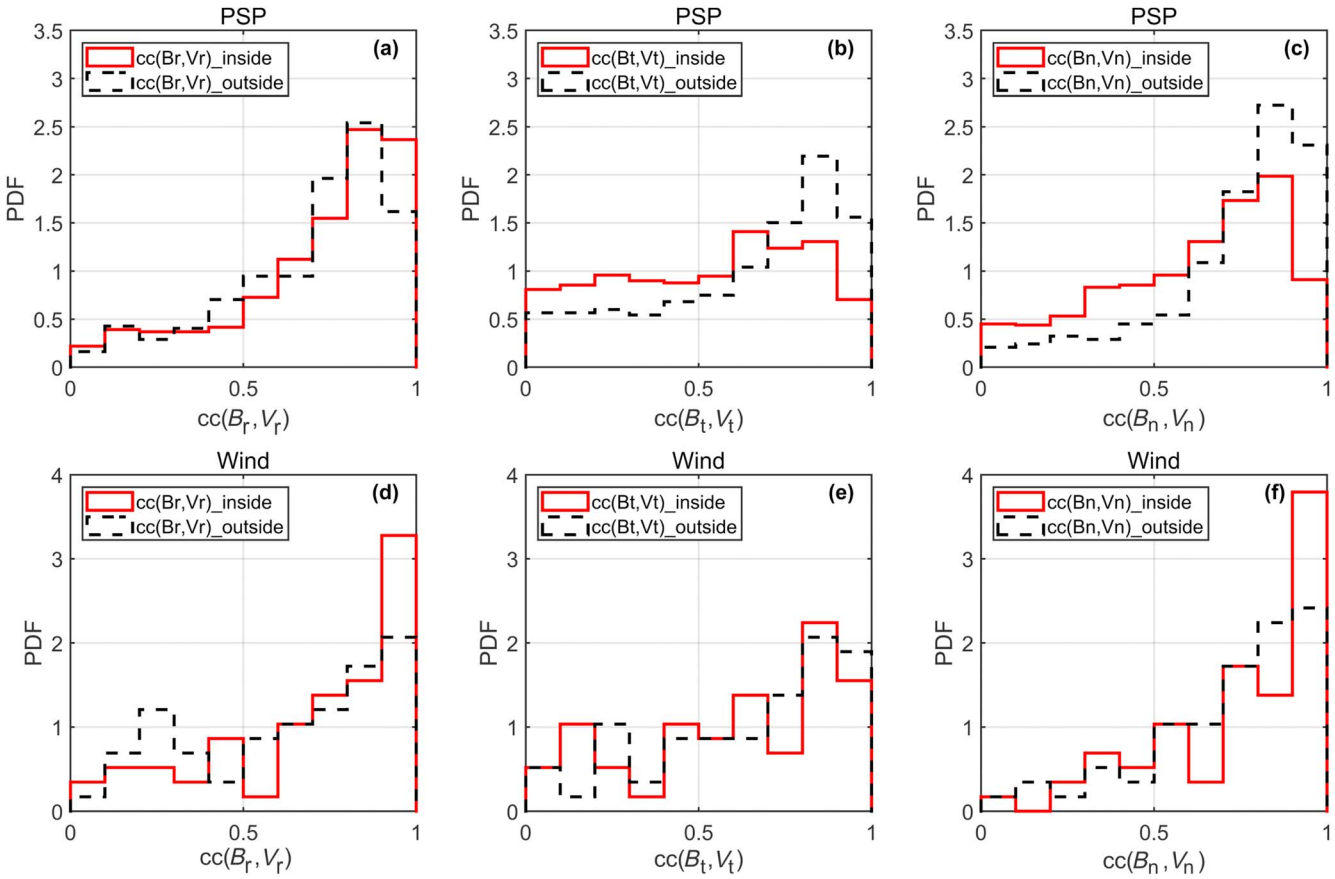

Figure 5. Probability distribution functions (PDFs) of correlation coefficients between the magnetic field and the velocity components in RTN coordinates. The red solid and black dashed histograms represent the PDFs inside and outside the kinks, respectively.

convection (Matteini et al. 2014; Squire et al. 2020). In our statistical results (Figure 6), kinks with boundaries of the RD-type take up a higher proportion.

In Figures 7(a) and (b), we classify the kink events into quasi-parallel and quasi-perpendicular events by θ_{Bn}. Quasi-parallel events can originate from the steepening of Alfvén pulses propagating parallel to the background magnetic field. However, parameters such as θ_{Bn}, β, and T_i/T_e, can affect the stability of the RDs, where β is the ratio of the thermal pressure to the magnetic pressure and T_i/T_e is the ratio of the proton-to-electron temperature (Vasquez & Cargill 1993). It is thus difficult to find a wide range of parameters that form stable quasi-parallel RDs (Vasquez & Cargill 1993). A possible reason for the instability of quasi-parallel RDs is the dispersion of Alfvén/ion-cyclotron modes with different wavenumbers near the RD boundary layer (Vasquez & Hollweg 1998). To keep quasi-parallel RDs stable, Vasquez & Hollweg (1998) find that the initial Alfvén waves after a modulation keep RDs stable over a large range of parameters (e.g., θ_{Bn}, β, T_i/T_e). The modulation is achieved by adding a fluctuation, which propagates quasi-parallel to the background magnetic field and perturbs in the third direction other than the direction of Alfvén wave propagation and Alfvén wave perturbation (Vasquez & Hollweg 1998). The quasi-parallel propagating Alfvén waves alone launched by the irregular motion in the photosphere cannot create such a modulation, and thus it is difficult to form stable quasi-parallel kink events of the RD type. Recent numerical simulations show that interchange magnetic reconnection can excite Alfvén waves to undergo the modulation process introduced by Vasquez & Hollweg (1998). In the simulation work of He et al. (2021), interchange reconnection excites fast-mode waves in addition to Alfvén waves, and the perturbation direction of the fast-mode waves satisfies the modulation conditions proposed by Vasquez & Hollweg (1998). Based on the work of Vasquez & Hollweg (1998) and He et al. (2021), the coupling of Alfvén waves and fast-mode waves excited by interchange reconnection (Zank et al. 2020) may jointly contribute to the formation of quasi-parallel kink events of the RD type.

Simulations show that Alfvén waves propagating quasi-perpendicular to the magnetic field can easily evolve into stable quasi-perpendicular RDs when $T_i/T_e > 0.1$ (Richter & Scholer 1989; Vasquez & Hollweg 1996, 1998). For the development of quasi-perpendicular RD-type kink events, Alfvén waves do not need to be modulated with additional fast-mode waves. The expanding solar wind model of Mallet et al. (2021) suggests that quasi-perpendicular Alfvén waves are more likely to form switchback structures. Alfvén waves formed by the transverse oscillation of magnetic field line footpoints in the photosphere can contribute to the quasi-perpendicular RD-type kink events when they propagate upward in flux tubes, which are nonuniform and adjacent. The increased stability of quasi-perpendicular RDs explains the slower decrease of quasi-perpendicular kink occurrences with increasing heliocentric distance (Figure 7(c)). Moreover, this concept is also consistent with the higher proportion of RD-type kinks at larger θ_{Bn} seen in Figure 7(d).

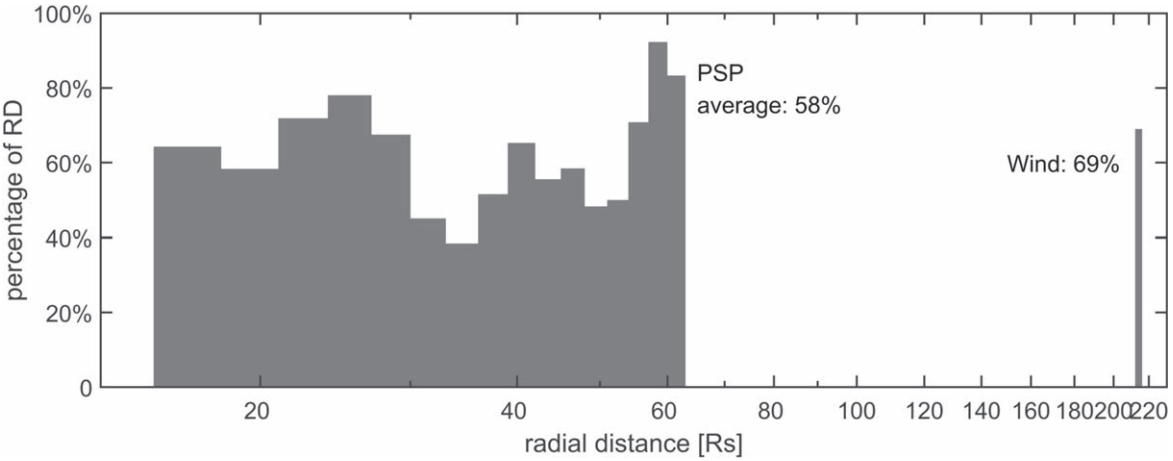

Figure 6. Percentages of RD-type kinks at different heliocentric distances.

Since the fast-mode waves and Alfvén waves excited by interchange magnetic reconnection, as shown by He et al. (2021), satisfy the above modulation process, we conjecture that interchange magnetic reconnection makes a more significant contribution to the formation of quasi-parallel RD-type kinks. In contrast, the sources of quasi-perpendicular Alfvén waves are not constrained. Therefore, various mechanisms that excite Alfvén waves can be responsible for quasi-perpendicular RD-type kinks (e.g., interchange magnetic reconnection and magnetic field line oscillations due to photospheric convection). In Figure 7(a), we see significantly more quasi-parallel kink events than quasi-perpendicular kink events, which suggests a more significant contribution of interchange magnetic reconnection to the origin of kinks.

Mozer et al. (2021) find that the switchback rate is independent of heliocentric distance and interpret this finding as indicative of a near-Sun source of the magnetic field kinks. In our case, the similar PDF of measurement points (Figure 1(b)) and the PDF of the kinks (Figure 3) confirms the independence of the kink rate with heliocentric distance in the inner heliosphere, which likewise suggests a near-Sun origin of kinks. A distribution of Alfvén waves (kink waves in the case of weak compressibility) with different amplitudes and periods can be excited by a variety of mechanisms: for example, by magnetic reconnection in the solar atmosphere or by transverse motions of the field line footpoints in the photosphere. These Aflvén waves (kink waves), during their outward propagation, may steepen to form magnetic kinks (even switchbacks) with varying rotation angles (Squire et al. 2020; Johnston et al. 2022). PSP is likely to observe a mix of these kinks and no clear dependence between rotation angles and heliocentric distance. Further detailed studies are required to determine the relationship between rotation angles and the origin mechanisms of kinks, which is beyond the scope of the present work.

The fitted curves in Figures 3(a) and (c) show that the velocity perturbation of the kinks is significantly lower than predicted by WKB theory and that the proton temperature inside the kinks increases with decreasing heliocentric distance. This finding suggests that there is significant energy dissipation inside the kinks during their outward propagation and that the region of enhanced dissipation is concentrated within 0.25 au. Based on the Alfvénic nature of the kinks and the success of the turbulent energy cascade model of Tu & Marsch (1995) in explaining the decay of Alfvén wave amplitudes in the solar wind, we hypothesize that the Alfvénic kinks observed by PSP, as an important part of the solar wind turbulence, are likely to participate in the cascade and dissipation of turbulent energy during their outward propagation. The energy cascade process usually arises from the nonlinear interaction between Alfvén waves propagating in opposite directions or between Alfvén waves and inhomogeneous 2D structures. The presence of actively cascading turbulent fluctuations reduces the correlation between the magnetic field and velocity (i.e., Alfvénicity). Figure 5, comparing the distributions of PSP kinks and WIND kinks, suggests that kinks with low Alfvénicity are more likely to dissipate during outward propagation, which is consistent with the expectation that non-purely-Alfvénic turbulence works actively to cascade energy to dissipation at kinetic scales. - Bourouaine et al. (2020) find that the turbulence inside kinks is more balanced in terms of Elsässer variables, supporting the idea of a more active cascade process inside kinks. The turbulent energy cascade to proton and sub-proton scales may be favorable for generating nonlinear ion-acoustic waves, ion holes, and electron holes that heat electrons and protons (Mozer et al. 2021). Recent work suggests that abundant kinetic Alfvén waves near kinks can contribute to the heating of protons (Malaspina et al. 2022). Huang et al. (2020) report that slow solar wind, which has not yet been fully accelerated within 0.25 au, experiences additional significant heating within 0.25 au. Moreover, Wu et al. (2020) find a significantly higher heating rate within 0.25 au than at larger distances. Since kink dissipation seems also concentrated within 0.25 au, these observations support the scenario that kink dissipation is an essential ingredient of turbulence dissipation within 0.25 au.

5. Summary

We statistically analyze kink events during nine solar encounters of PSP and compare them with the properties of kinks observed by WIND at 1 au. Concerning the kink nature, origin, and dissipation, we identify the following conclusions:

1. We find similar high Alfvénicity inside and outside the kinks, suggesting a connection between the kinks and Alfvén waves. These kinks can originate from the steepening of Alfvén waves, with each wave train corresponding to a cluster of switchbacks.

2. Kinks can be classified into two categories based on their angles between the normal direction of their boundaries and the

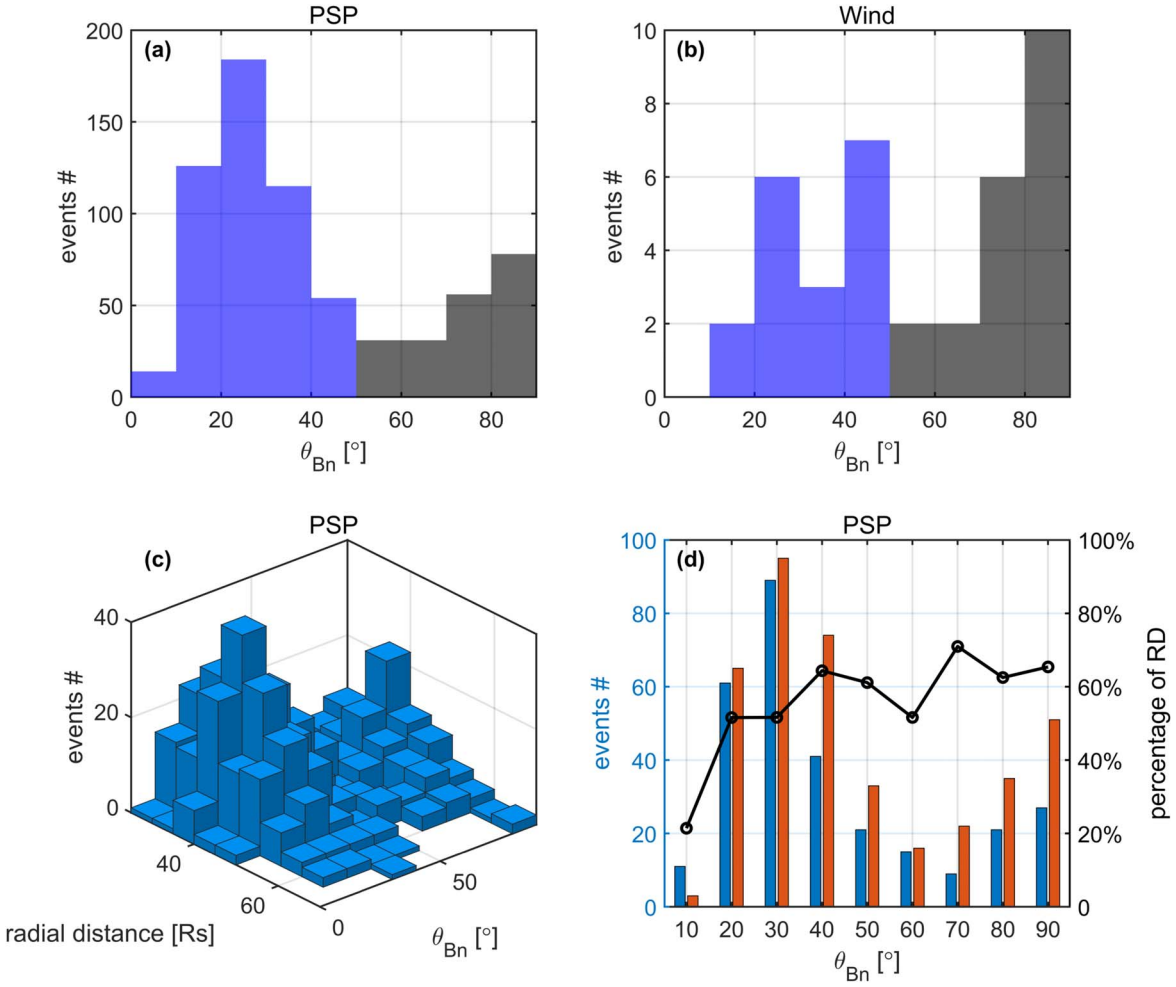

Figure 7. (a) Histogram of the angle between the background magnetic field and the normal direction of the PSP-kink boundaries. (b) Histogram of the angle between the magnetic field and the normal direction of the WIND-kink boundaries. Blue and gray colors indicate our classification of the kinks into the two groups. (c) Histogram of PSP kinks in the 2D space of θ_{Bn} and heliocentric distance. (d) Histograms of the angle between the background magnetic field and the boundary normal direction of RD-type (red histograms) and non-RD-type (blue histograms) kinks, with the histogram heights marked on the left axis. The solid line represents the percentage of RD-type kinks with values marked on the right axis.

background magnetic field: quasi-parallel kinks and quasi-perpendicular kinks, where a larger proportion of PSP kinks are in the quasi-parallel category. Combining the simulation work of Vasquez & Hollweg (1998) and He et al. (2021), we conjecture that the quasi-parallel RD-type kinks mainly originate from the steepening of coupled Alfvén waves and fast-mode waves excited by coronal interchange magnetic reconnection. Both interchange magnetic reconnection and magnetic field line oscillations may contribute to the formation of quasi-perpendicular RD-type kinks. Due to the higher number of observed quasi-parallel RD-type kinks, interchange magnetic reconnection may be the primary mechanism for kink formation. In contrast, background Alfvén waves in the corona not related to interchange reconnection may be responsible for a relatively small fraction of kinks.

3. Outward-propagating kinks exhibit decreasing amplitudes in their velocity spikes with respect to the local background Alfvén speed, mainly within 0.25 au, suggesting a possibly significant dissipation of these kinks within 0.25 au. The temperature inside the kinks is almost always greater than the temperature outside, which is also consistent with the dissipative heating of plasma in the kinks. The energy source for this dissipative heating is potentially linked to the transition of the Alfvénic kinks to kinetic Alfvén fluctuations due to their merging with the turbulent cascade.

Acknowledgments

The work at Peking University is supported by National Key R&D Program of China (2021YFA0718600 and 2022YFF0503800), by NSFC (42241118, 42174194, 42150105, and 42204166), and by CNSA (D020301 and D050106). D.V. from UCL is supported by the STFC Ernest Rutherford Fellowship ST/P003826/1 and STFC Consolidated Grants ST/S000240/1 and ST/W001004/1. C.H. from Peking University is also supported by the China Scholarship Council (202206010136). D.D. from Peking University is also supported by China Postdoctoral Science Foundation (2022M720213). The authors would like to declare that Chuanpeng Hou, Xingyu Zhu, and Rui Zhuo contributed equally to this work and should be considered co-first authors. The authors acknowledge the contributions of the Parker Solar Probe mission operations and spacecraft engineering teams at the Johns Hopkins University Applied Physics Laboratory as well as the FIELDS, SWEAP, and SPAN teams for the use of the data. The authors thank the 3DP team and MFI team on WIND for sharing data. PSP and WIND data are available on SPDF (https://cdaweb.gsfc.nasa.gov).

ORCID iDs

Chuanpeng Hou https://orcid.org/0000-0001-7205-2449
Xingyu Zhu https://orcid.org/0000-0002-1541-6397
Rui Zhuo https://orcid.org/0000-0003-4726-9755
Jiansen He https://orcid.org/0000-0001-8179-417X
Daniel Verscharen https://orcid.org/0000-0002-0497-1096
Die Duan https://orcid.org/0000-0002-6300-6800

References

Bale, S. D., Badman, S. T., Bonnell, J. W., et al. 2019, Natur, 576, 237
Bale, S. D., Goetz, K., Harvey, P. R., et al. 2016, SSRv, 204, 49
Bourouaine, S., Perez, J. C., Klein, K. G., et al. 2020, ApJL, 904, L30
Dudok de Wit, T. D., Krasnoselskikh, V. V., Bale, S. D., et al. 2020, ApJS, 246, 39
Farrell, W. M., MacDowall, R. J., Gruesbeck, J. R., Bale, S. D., & Kasper, J. C. 2020, ApJS, 249, 28
Fisk, L., & Kasper, J. 2020, ApJL, 894, L4
Froment, C., Krasnoselskikh, V., Dudok de Wit, T., et al. 2021, A&A, 650, A5
Gosling, J., McComas, D., Roberts, D., & Skoug, R. 2009, ApJL, 695, L213
He, J., Zhu, X., Yang, L., et al. 2021, ApJL, 913, L14
Horbury, T., Matteini, L., & Stansby, D. 2018, MNRAS, 478, 1980
Horbury, T. S., Woolley, T., Laker, R., et al. 2020, ApJS, 246, 45
Huang, J., Kasper, J. C., Vech, D., et al. 2020, ApJS, 246, 70
Johnston, Z., Squire, J., Mallet, A., & Meyrand, R. 2022, PhPl, 29, 072902
Kasper, J. C., Abiad, R., Austin, G., et al. 2016, SSRv, 204, 131
Kasper, J. C., Bale, S. D., Belcher, J. W., et al. 2019, Natur, 576, 228
Larosa, A., Krasnoselskikh, V., Dudok de Wit, T., et al. 2021, A&A, 650, A3
Lepping, R., Acũna, M., Burlaga, L., et al. 1995, SSRv, 71, 207
Liang, H., Zank, G. P., Nakanotani, M., & Zhao, L. L. 2021, ApJ, 917, 110
Lin, R., Anderson, K., Ashford, S., et al. 1995, SSRv, 71, 125
Liu, Y. Y., Fu, H. S., Cao, J. B., et al. 2022, JGRA, 127, e29983
Malaspina, D. M., Chasapis, A., Tatum, P., et al. 2022, ApJ, 936, 128
Mallet, A., Squire, J., Chandran, B. D. G., Bowen, T., & Bale, S. D. 2021, ApJ, 918, 62
Matteini, L., Horbury, T. S., Neugebauer, M., & Goldstein, B. E. 2014, GeoRL, 41, 259
Mozer, F. S., Agapitov, O. V., Bale, S. D., et al. 2020, ApJS, 246, 68
Mozer, F. S., Bale, S., Bonnell, J., et al. 2021, ApJ, 919, 60
Mozer, F. S., Bonnell, J. W., Hanson, E. L. M., Gasque, L. C., & Vasko, I. Y. 2021, ApJ, 911, 89
Richter, P., & Scholer, M. 1989, GeoRL, 16, 1257
Ruffolo, D., Matthaeus, W. H., Chhiber, R., et al. 2020, ApJ, 902, 94
Schwadron, N., & McComas, D. 2021, ApJ, 909, 95
Shi, C., Panasenco, O., Velli, M., et al. 2022, ApJ, 934, 152
Sonnerup, B. U. Ö., & Scheible, M. 1998, in Analysis Methods for Multi-Spacecraft Data, ed. Bengt U. Ö. Götz & M. Scheible, 1 (Noordwijk: ESA Publications Division), 185
Squire, J., Chandran, B. D., & Meyrand, R. 2020, ApJL, 891, L2
Tenerani, A., Velli, M., Matteini, L., et al. 2020, ApJS, 246, 32
Tsurutani, B., Ho, C., Smith, E., et al. 1994, GeoRL, 21, 2267
Tu, C.-Y., & Marsch, E. 1995, SSRv, 73, 1
Vasquez, B. J., & Cargill, P. J. 1993, JGRA, 98, 1277
Vasquez, B. J., & Hollweg, J. V. 1996, JGR, 101, 13527
Vasquez, B. J., & Hollweg, J. V. 1998, JGR, 103, 349
Wang, X., Tu, C., He, J., Marsch, E., & Wang, L. 2013, ApJL, 772, L14
Whittlesey, P. L., Larson, D. E., Kasper, J. C., et al. 2020, ApJS, 246, 74
Woodham, L. D., Horbury, T. S., Matteini, L., et al. 2021, A&A, 650, L1
Wu, H., Tu, C., Wang, X., He, J., & Yang, L. 2020, ApJL, 904, L8
Yang, L., Zhang, L., He, J., et al. 2015, ApJ, 809, 155
Zank, G., Nakanotani, M., Zhao, L.-L., Adhikari, L., & Kasper, J. 2020, ApJ, 903, 1